RSC Advances

ROYAL SOCIETY OF CHEMISTRY

www.rsc.org/advances

Graphical Abstract Figure

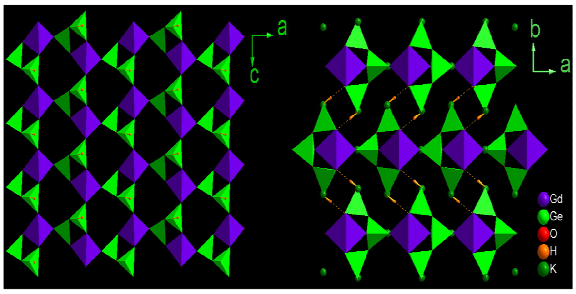

Graphical Abstract Legend

A family of new lanthanide germanates $K_3Ln_2Ge_3O_8$ $(OH)_2$ have been synthesized by a High-temperature, high-pressure hydrothermal method and characterized by single-crystal X-ray diffraction, IR spectra, Energy-dispersive spectroscopy (EDS).

Cite this: DOI: 10.1039/c0xx00000x

www.rsc.org/xxxxxx

ARTICLE TYPE

High-Temperature, High-Pressure Hydrothermal Synthesis, Crystal Structure and Photoluminescent Properties of $K_3[Gd_{1-x}Tb_xGe_3O_8(OH)_2]$ (x = 0, 0.3, 0.1, 1)

Wei Liu, Min Yang, Ying Ji, Fuyang Liu, Ying Wang, Xiaofeng Wang, Xudong Zhao* and Xiaoyang Liu*

Received (in XXX, XXX) Xth XXXXXXXXX 20XX, Accepted Xth XXXXXXXXX 20XX
DOI: 10.1039/b000000x

A family of 2D-layered lanthanide germanates $K_3[Gd_{1-x}Tb_xGe_3O_8(OH)_2]$ (x = 0, 0.3, 0.1, and 1), have been synthesized by a high-temperature, high-pressure hydrothermal method and characterized by single-crystal X-ray diffraction, photoluminescence, IR spectra, and Energy-dispersive spectroscopy (EDS). The X-ray powder diffraction patterns of these compounds reveal that they are isostructural. The single-crystal X-ray diffraction analysis of $K_3[GdGe_3O_8(OH)_2]$ reveals that it is 2D-layered $[LnGe_3O_8(OH)_2]_n^{3n-}$ anionic framework which is built up from GeO_4H/GeO_4 tetrahedra and GdO_6 octahedra by sharing vertex O atoms. K^+ ions locate in the free void space to achieve the charge balance of the framework. Sample containing only Tb^{3+} emit mainly from one transition, $^5D_4 \rightarrow {}^7F_5$ (552 nm). Mixed lanthanide samples, $K_3[Gd_{1-x}Tb_xGe_3O_8(OH)_2]$ (x = 0.3, and 0.1), have also been prepared and efficient Gd → Tb energy transfer has been observed.

1. Introduction

In recent years, lanthanide-containing silicates and germanates have been attracting much interest because of their rich structural chemistry and potential applications in optical materials.[1,2] The use of silicates and germanates as host materials permits obtaining phosphors with superior color richness and excellent chemical and thermal stability.[3-6] In the past decades, many lanthanide silicates that are built from SiO_4 tetrahedra and LnOn ($n \geqslant 6$) polyhedral have been successfully synthesized under mild hydrothermal conditions in Teflon-lined stainless steel autoclaves in the temperature range of 100-240˚C. For instance, the first cerium silicate $Na_4K_2Ce_2Si_{16}O_{38}\cdot 10H_2O$ (AV-5) was reported by Rocha and co-workers under mild hydrothermal conditions at 503K in 2000.[7] Since then, a series of lanthanide silicates AV-n (n = 9, 20, 22, 23) have been successfully prepared under mild hydrothermal conditions, their structures and fine-tuning luminescent properties derived from the multiple Ln^{3+} ions have also been investigated.[8-11] High-temperature and high-pressure hydrothermal synthetic method has also been used in exploratory syntheses of transition metals,[12,13] lanthanide elements,[14,15] and uranium-based[16-19] silicates because of the important roles of high pressure in the synthetic chemistry.[20]

However, in contrast to the lanthanide silicates, much less work has been reported on the germanium analogues. Unlike the lanthanide silicates， most lanthanide germanates are dense phases and comprised of anionic groups[21-23] that are further connected via LnOn ($n \geqslant 6$) polyhedra. In 2007, Pei-Lin Chen *et al*. reported a new Eu(III) germanate $KEuGe_2O_6$ with parallel zigzag chains of edge-sharing Eu-O polyhedra synthesized by both the flux-growth method and the high-temperature, high-pressure hydrothermal method.[24] Recently, Lii and co-workers reported a number of uranium germanates prepared by high-temperature and high-pressure hydrothermal synthetic method and investigated their crystal structure as well as luminescence properties.[25-28] Importantly, these compounds mentioned above can not be obtained under mild hydrothermal conditions.

In this work, we report a family of new lanthanide germanates $K_3[Gd_{1-x}Tb_xGe_3O_8(OH)_2]$ (x = 0, 0.3, 0.1, and 1), which are synthesized by high-temperature and high-pressure hydrothermal synthetic method at 400℃ and 100MPa. Their structures are closely related to $K_3LnSi_3O_8(OH)_2$ (Ln = Y^{3+}, Eu^{3+}, Tb^{3+}, Er^{3+}; denoted as AV-22)[10] that were prepared under the mild hydrothermal conditions at 230℃ for 7 days. The luminescent property and energy transfer from Gd^{3+} to Tb^{3+} in $K_3[Gd_{1-x}Tb_xGe_3O_8(OH)_2]$ (x = 0.3, and 0.1) have been studied as well.

2. 2. Experimental Section

2.1. Materials and synthesis

High-temperature, high-pressure hydrothermal synthesis was carried out under autogenous pressure in silver tube contained in a hydrothermal research system (Model HR-1B-2, LECO Tem-Pres), where pressure was provided by water. Typically, a reaction mixture of 0.246 g of KOH (Beijing chemical plant), 0.132 g of GeO_2 (Alfa Aesar, 99.99%), 0.0788g of $Gd(NO_3)\cdot 6H_2O$ (Alfa Aesar, 99.995%) or 0.079 g of terbium nitrate hexahydrate (Alfa Aesar, 99.995%), and 0.1 ml of deionized water (molar ratio K:Gd:Ge:H_2O = 7:1:0.14:4.3) in a 5.0 cm long silver tube (inside diameter = 4.90 mm) was heated at 400 ℃ for 5 h. The pressure was initially increased to 120 MPa and maintained until the temperature was increased to 400˚C. Then the pressure was maintained at 100 MPa. After reaction, the

autoclave was then fast cooled to room temperature by removing the autoclave from the furnace. The resulting colorless crystals were filtered, washed with deionized water, and dried at 353 K. The Gd^{3+}/Tb^{3+} mixed samples were prepared by introducing the desired Gd^{3+} and Tb^{3+} contents in the initial mixture.

2.2. Characterizations

Powder X-ray diffraction (XRD) data were collected using a Rigaku D/Max 2550 V/PC X-ray diffractometer with graphite-monochromated Cu Kα radiation (λ = 0.15418 nm) at 50 kV and 200mA at room temperature. IR spectra were recorded on a Nicolet Impact 410 FT-IR spectrometer using the KBr pellet technique. Energy-dispersive spectroscopy (EDS) analysis was carried out using an EDS system with a window attached to a JEOL JSM-6700F scanning electron microscope. The photoluminescence (PL) spectra were obtained on a FlouroMax-4 spectrophotometer with Xe 900 (150 W xenon arc lamp) as the light source. To eliminate the second-order emission from the source radiation, a cut-off filter was used during the measurement. The PL decay curves were measured on an FLS920 spectrophotometer (Edinburgh Instruments) with a μF920H flash lamp as the light source. Slit widths were 0.20 (excitation) and 0.20 (emission) nm. All spectra were recorded at room temperature.

2.3. Single-crystal Structure Determination

Suitable single crystals of $K_3[GdGe_3O_8(OH)_2]$, and $K_3[TbGe_3O_8(OH)_2]$ with dimensions of 0.12 x 0.06 x 0.04 mm and 0.16 x 0.08 x 0.05 mm, respectively, were selected for single-crystal X-ray diffraction analysis. Intensity data collection were collected on a Bruker SMART APEX 2 micro-focused diffractometer using graphite-monochromated Mo Kα radiation (λ = 0.71073 nm) at 50kV and 0.6 mA at a temperature of 296 K. Data processing was accomplished with the APEX 2 processing program. The structures were solved by direct methods and refined by full-matrix least-squares techniques with the SHELXTL crystallographic software package.[29] All heaviest atoms, K, Gd, and Ge for $K_3[GdGe_3O_8(OH)_2]$, K, Tb, and Ge for $K_3[TbGe_3O_8(OH)_2]$, were unambiguously located in the Fourier maps, and then O atoms were found in the subsequent difference Fourier maps. The H atoms attached to the GeO_4 tetrahedron were placed geometrically. All atoms were refined with anisotropic displacement parameters, except for H atoms, which were refined with an isotropic thermal displacement parameter (Uiso) fixed at 1.5*U*eq of the parent O atoms. The final cycles of least-squares refinement including atomic coordinates and anisotropic thermal parameters for all atoms converged at $R_1 = 0.0174$, $wR_2 = 0.0428$, and S=1.104 for $K_3[GdGe_3O_8(OH)_2]$; $R_1 = 0.0195$, $wR_2 = 0.0444$, and S=1.064 for $K_3[TbGe_3O_8(OH)_2]$; A summary of the crystallographic data is presented in Table 1. The selected bond lengths [Å] and angles [deg] for $K_3[GdGe_3O_8(OH)_2]$, and $K_3[TbGe_3O_8(OH)_2]$ are presented in Table S1 and table S2, atomic coordinates and equivalent isotropic displacement parameters are presented in table S3 and table S4 (Supporting Information).

Table 1 Crystal Data and Structure Refinement for $K_3[LnGe_3O_8(OH)_2]$(Ln = Gd, Tb)

Empirical formula	$K_3GdGe_3O_8(OH)_2$	$K_3Tb\ Ge_3O_8(OH)_2$
Formula weight	654.34	656.01
Temperature (K)	293(2)	293(2)
Wavelength (Å)	0.71073	0.71073
Crystal system, space group	Orthorhombic, *P*nma	Orthorhombic, *P*nma
Unit cell dimensions	a = 13.6880(7) Å, α = 90 °C b = 13.6891(7) Å, β = 90 °C c = 6.0821(3) Å , γ = 90 °C	a = 13.6552(15) Å, α = 90 °C b = 13.6541(15) Å , β = 90 °C c = 6.0595(6) Å , γ = 90 °C
Volume ($Å^3$)	1139.64(10)	1129.8(2)
Z, Calculated density (Mg/m^3)	4, 3.814	4, 3.857
Crystal size (mm^3)	0.12 x 0.06 x 0.04	0.16 x 0.08 x 0.05
Absorption coefficient (mm^{-1})	14.712	15.230
F(000)	1196	1200
Theta range for data collection	2.98 ~ 26.35 °	2.98 ~ 26.35
Completeness to theta = 26.35	100.0 %	100.0 %
Max. and min. transmission	0.555 and 0.498	0.737 and 0.701
Goodness-of-fit on F^2	1.104	1.064
Final R indices [I>2sigma(I)]	$R_1 = 0.0162$, $wR_2 = 0.0423$	$R_1 = 0.0186$, $wR_2 = 0.0439$
R indices (all data)	$R_1 = 0.0174$, $wR_2 = 0.0428$	$R_1 = 0.0195$, $wR_2 = 0.0444$
Largest diff. peak and hole	1.069 and -1.063 e. $Å^{-3}$	0.945 and -1.429 e. $Å^{-3}$

3. Results and Discussion

3.1. Characterization

Unlike the lanthanide silicates hydrothermally prepared by using an excess amount of water as the solvent, single crystals of these lanthanides germanates could be only obtained in a concentrated gel system with a low H_2O/GeO_2 molar ratio. Interestingly, single crystals of $Ln_2Ge_2O_7$ were obtained when the H_2O/GeO_2 molar ratio exceeds the ratio used in the experiment.

The X-ray powder diffraction patterns of the four compounds are shown in Figure 1, which are consistent with the simulated one on the basis of single-crystal structural analysis, indicating that they are isostructural. The energy-dispersive spectroscopy (EDS) analysis results of the four compounds are displayed in Table S5 and Figure S1 in the Supporting Information, which are in agreement with the values given by the theoretically calculated values.

3.2. Description of the structure

The four compounds are isostructural, therefore, only the structure of $K_3[GdGe_3O_8(OH)_2]$ is discussed. The structure of $K_3[GdGe_3O_8(OH)_2]$ crystallizes in the *P*nma space group (No. 62) with a = 13.6880(7) Å, b = 13.6891(7) Å, and c = 6.0821(3) Å, that is analogous to some lanthanide silicates $K_3LnSi_3O_8(OH)_2$ (Ln = Y^{3+}, Eu^{3+}, Tb^{3+}, Er^{3+}; denoted as AV-22). Figure 2 shows the asymmetric units of $K_3[GdGe_3O_8(OH)_2]$. The structure is constructed from the following building units: 2 K^+ cations, 1 GdO_6 octahedra, 1 GeO_4 tetrahedra, and 1 GeO_4H tetrahedra. GdO_6 is discrete and is distorted with the Gd-O bond lengths in the range from 2.226(4) to 2.332(3) Å.

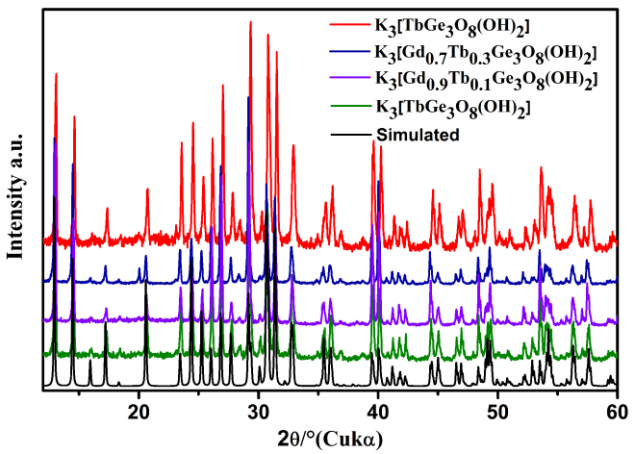

Fig.1 Simulated powder XRD pattern of $K_3[GdGe_3O_8(OH)_2]$ and experimental XRD patterns of the as synthesized four compounds

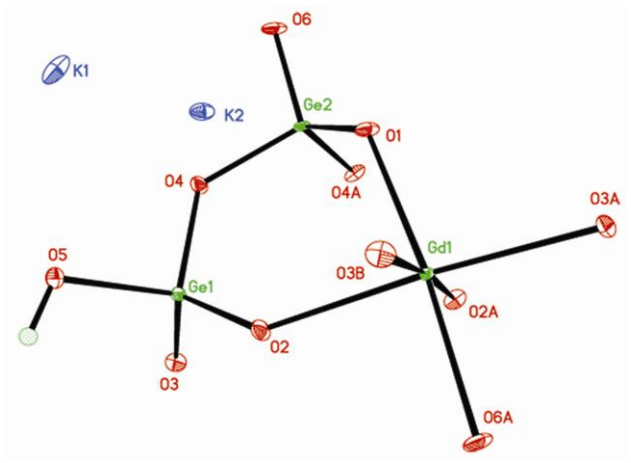

Fig.2 Thermal ellipsoid plot (50% probability) of the asymmetric unit of $K_3[GdGe_3O_8(OH)_2]$

The existence of Ge−O bonds and an −OH group is confirmed by IR analysis (Figure S2). The peaks at 810, 781, and 760 cm^{-1} can be assigned to the asymmetric stretching vibrations of the Ge−O bonds, and the bands at about 3000cm^{-1} correspond to the −OH groups. On the basis of the maximum cation-anion distance by Donnay and Allmann,[30] a limit of 3.35 Å was set for K-O interactions, which gives the following coordination numbers: K(1), 5-coordinate [K(1)-O, 2.808(3)-3.063(2) Å]; K(2), 9-coordinate [K(2)-O, 2.694(3) - 3.281(3) Å].

The crystal structure analysis of $K_3[GdGe_3O_8(OH)_2]$ reveals that it is a 2D-layered $[GdGe_3O_8(OH)_2]_n^{3n-}$ anionic framework, which is built up from GeO_4H/GeO_4 tetrahedra and GdO_6 octahedra by sharing vertex O atoms. As can be seen in Figure 3a, The GeO_4 tetrahedra, GeO_4H tetrahedra and GdO_6 octahedra are connected together by sharing corners to form a single layer in the (010) plane with the composition $GdGe_3O_8(OH)_2$ containing 3, and 7-rings. Adjacent layers are interconnected through the O−H ··O hydrogen bonds [O(5)−H(1), 0.820 Å; H(1) ··O(2), 1.860 Å; O(6) ··O(3), 2.671 Å] between the neighboring Ge−OH groups, and stacked in the sequence of [ABAB…] in the (001) plane (Figure 3b). K(1) ions are arranged in the interlayer space, while K(2) ions are located in the seven-ring windows.

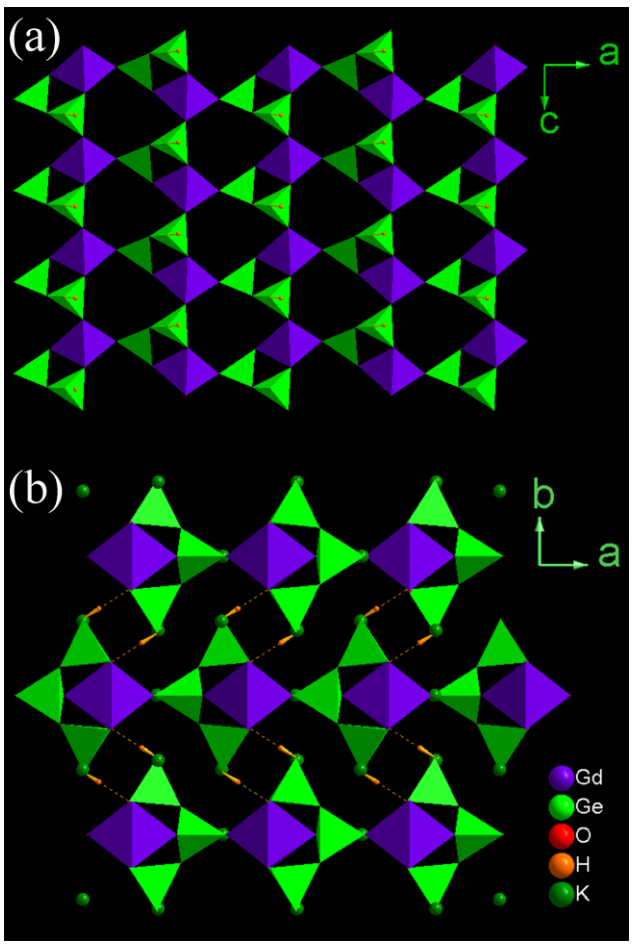

Fig.3 (a) Single layer with three and seven rings viewed along the [010] direction. (b) Polyhedral view of $K_3[GdGe_3O_8(OH)_2]$ along the [001] direction. Colour code: Gd, Purple; Ge, bright green; K, green; O, red; H, orange

3.3. Photoluminescence property

Figure 4 shows the room temperature (RT) excitation spectra of $K_3[Gd_{1-x}Tb_xGe_3O_8(OH)_2]$ for x = 0.1 , 0.3 and 1 (pure Tb^{3+}

sample), monitored within the $^5D_4 \rightarrow {}^7F_5$ transition (542 nm). In the excitation spectrum of $K_3[TbGe_3O_8(OH)_2]$, the sharp lines between 300 and 500 nm are assigned to $^7F_6 \rightarrow {}^5D_{0,1}$, $^7F_6 \rightarrow {}^5G_{2\text{-}6}$, $^5L_{10}$, and $^7F_6 \rightarrow {}^5D_{3,4}$ transitions of Tb^{3+}. The broad band between 250 and 300 nm is ascribed to the spin-forbidden (high-spin) interconfigurational $^4f_8 \rightarrow {}^4f_7{}^5d^1$ transition.[31,32] The excitation spectra monitored at the main $^5D_4 \rightarrow {}^7F_5$ transition (542 nm) of $K_3[Gd_{1-x}Tb_xGe_3O_8(OH)_2]$ for x = 0.1, 0.3 (Figure 4) display the same Tb^{3+} lines. In addition, the excitation lines at 274 nm and 312 nm due to transitions from $^8S_{7/2} \rightarrow {}^6I_{9/2}$, and $^8S_{7/2} \rightarrow {}^6P_{7/2}$ of Gd^{3+} ion can be observed. This is clear evidence for Gd^{3+}-to-Tb^{3+} energy transfer. Furthermore, the Gd^{3+}-to-Tb^{3+} energy transfer is also detected in the emission of the $K_3[Gd_{1-x}Tb_xGe_3O_8(OH)_2]$ (x=0.3, and 0.1) samples (Figure 5).[10,33-35]

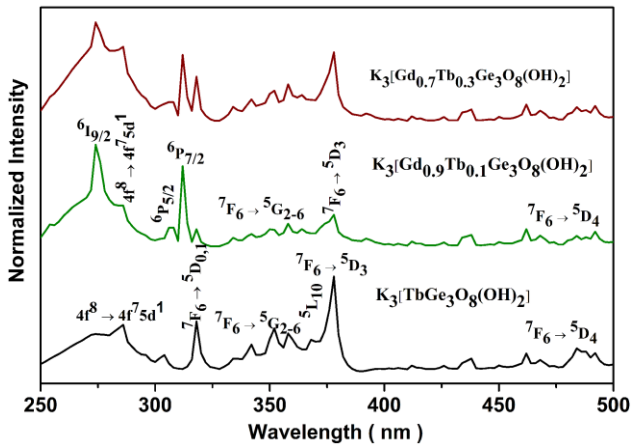

Fig.4 RT excitation spectra of $K_3[Gd_{1x}Tb_xGe_3O_8(OH)_2]$ for x = 0.1 , 0.3 and 1 (λ_m = 542 nm)

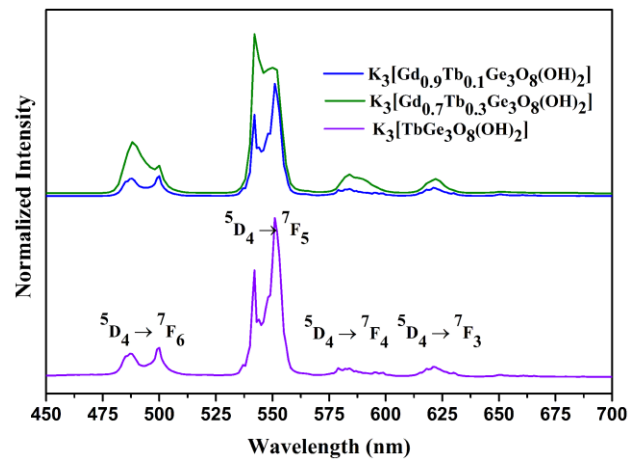

Fig.5 RT emission spectrum of $K_3[TbGe_3O_8(OH)_2]$ (λ_{ex} = 377), and $K_3[Gd_{1-x}Tb_xGe_3O_8(OH)_2]$ for x = 0.1, and 0.3 (λ_{ex} = 274)

Figure 5 shows the RT emission spectrum of $K_3[Gd_{1-x}Tb_xGe_3O_8(OH)_2]$ for x = 0.1, 0.3 and 1. The emission spectrum of $K_3[TbGe_3O_8(OH)_2]$ (pure Tb^{3+} sample) excited at 377 nm (Tb^{3+} $^5D_3$) displays a series of sharp lines from 475 to 675 nm, which are associated with the $^5D_4 \rightarrow {}^7F_{3\text{-}6}$ transitions of Tb^{3+} with the strongest at about 542 and 552 nm ($^5D_4 \rightarrow {}^7F_5$). Luminescence from the higher (e.g., $^5D_3$) excited states is not detected, even for the samples with the lowest Tb^{3+} content, indicating very efficient nonradiative relaxation to the $^5D_4$ level.

The emission spectrua of $K_3[Gd_{1-x}Tb_xGe_3O_8(OH)_2]$ for x = 0.1, and 0.3 excited at the Gd^{3+} $^6I_{9/2}$ level (274 nm) show the typical Tb^{3+} lines (present in the spectrum of the pure Tb^{3+} sample, Figure 5). This further supports the above mentioned energy transfer between Gd^{3+} and Tb^{3+}.[36,37]

The RT luminescence decay curves detected at the $^5D_4 \rightarrow {}^7F_5$ transition of $K_3[Gd_{1-x}Tb_xGe_3O_8(OH)_2]$ (x = 0.1, 0.3) are shown in Figure 6. Both of them can be well fitted by the single exponential equation: $I(t) = I_0 + A\exp(-t/\tau)$, where I and I_0 is the luminescence intensity, A the constant, t the time, τ the decay time, yielding the lifetime values of τ = 2.255 and 2.909 ms for x = 0.1 and x = 0.3, respectively. The results confirm the presence of one local Tn^{3+} environment, which is consistent with the asymmetric Tb^{3+} location according to structural analysis.[14,36]

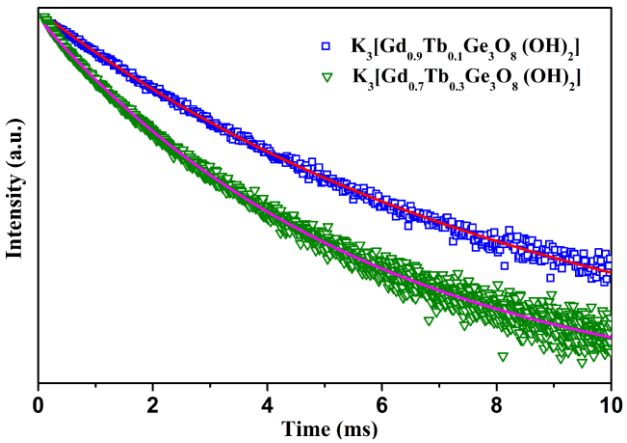

Fig.6 RT fluorescence decay curves detected at 542 nm (λ_{ex} = 276 nm) for $K_3[Gd_{1x}Tb_xGe_3O_8(OH)_2]$($x$ = 0.1, 0.3). The solid line represents the best fit to the data.

4. Conclusion

Four isostructural 2D-layered lanthanide germanates $K_3[Gd_{1-x}Tb_xGe_3O_8(OH)_2]$(x=0, 0.3, 0.1, 1), have been prepared by a High-temperature, high-pressure hydrothermal method at 400 ˚C for 5h. The crystal structure analyses reveal that they are built up from GeO_4H/GeO_4 tetrahedra and LnO_6 octahedra by sharing vertex O atoms, giving rise to a 2D-layered $[LnGe_3O_8(OH)_2]_n^{3n-}$ anionic framework. The energy transfer from Gd^{3+}-to-Tb^{3+} is observed in the excitation spectra of $K_3[Gd_{1-x}Tb_xGe_3O_8(OH)_2]$ (x = 0.1, 0.3) and confirmed by their emission spectra excited at the Gd^{3+} $^6I_{9/2}$ level (276 nm). The successful high-temperature, high-pressure hydrothermal synthesis of $K_3[LnGe_3O_8(OH)_2]$ will provide a new way to preparing many more novel lanthanide germanates.

Acknowledgements

This work was supported by the National Sciences Foundation of China (No.21271082, 21301066 and 21371068).

Notes and references

State Key Laboratory of Inorganic Synthesis and Preparative Chemistry, College of Chemistry, Jilin University, 2699 Qianjin Street, Changchun 130012, P. R. China; E-mail: liuxy@jlu.edu.cn ;
Fax: (+86) 431-85168316; Tel: (+86) 431-85168316

† Electronic Supplementary Information (ESI) available: [details of any supplementary information available should be included here]. See DOI: 10.1039/b000000x/

‡ Footnotes should appear here. These might include comments relevant to but not central to the matter under discussion, limited experimental and spectral data, and crystallographic data.

1 C. Feldmann, T. Jüstel, C.R. Rond, P.J. Schmidt, *Adv. Funct. Mater.*, 2003, **13**, 511.
2 B. M. van der Ende, L. Aartsa, A. Meijerink, *Phys. Chem. Chem. Phys,*. 2009, **11**, 11081.
3 A. Dobrowolska, E. Zych, *J. Solid State Chem.*, 2011, **184**, 1707.
4 K.V. Ivanovskikh, A. Meijerink, F. Piccinelli, A. Speghini, E.I. Zinin, C. Ronda, M. Bettinelli, *J.Lumin.*, 2010, **130**, 603.
5 P.L. Chen, P.Y. Chiang, H.C. Yeh, B.C. Chang, K.H. Lii, *Dalton Trans.*, 2008, 1721.
6 V.R. Bandi, Y.T. Nien, I.G. Chen, *J Appl. Phys.*, 2010, **108**, 023111.
7 J. Rocha, P. Ferreira, L. D. Carlos, A. Ferreira, *Angew.Chem.Int.Ed.*, 2000, **39**, 2174.
8 D. Ananias, A. Ferreira, J. Rocha, P. Ferreira, J. P. Rainho , C. Morais, L. D. Carlos, *J. Am. Chem. Soc.*, 2001, **123**, 5735.
9 A. Ferreira, D. Ananias, L.D. Carlos, C.M. Morais, J. Rocha, *J. Am. Chem. Soc.*, 2003, **125**, 14573.
10 D. Ananias, M. Kostova, F. A. Almeida Paz, A. Ferreira, L.D. Carlos, J. Klinowski, J. Rocha, *J. Am. Chem. Soc.*, 2004, **126**, 10410.
11 M.H. Kostova, D. Ananias, F.A. Almeida Paz, A. Ferreira, J. Rocha, L.D. Carlos, *J. Phys. Chem. B.*, 2007, **111**, 3576.
12 C.Y. Li, C.Y. Hsieh, H.M. Lin, H.M. Kao, K.H. Lii, *Inorg. Chem.*, 2002, **41**, 4206.
13 L.I Hung, S. Wang, S.P. Szu, C.Y. Hsieh, H.M. Kao, K.H. Lii, *Chem. Mater.*, 2004, **16**, 1660.
14 M.Y. Huang, Y.H. Chen, B.C. Chang, K.H. Lii, *Chem. Mater.*, 2005, **17**, 5743.
15 X.G. Zhao, J.Y. Li, P. Chen, Y. Li, Q.X. Chu, X.Y Liu, J.H. Yu, R.R. Xu, *Inorg. Chem.*, 2010, **49**, 9833.
16 C.S. Chen, H.M. Kao, K.H. Lii, *Inorg. Chem.*, 2005, **44**, 935.
17 C.S. Chen, R.K. Chiang, H.M. Kao, K.H. Lii, *Inorg. Chem.*, 2005, **44**, 3914.
18 C.S. Chen, S.F. Lee, K.H. Lii, *J. Am. Chem. Soc.*, 2005, **127**, 12208.
19 H.K. Liu, K.H. Lii, *Inorg. Chem.*, 2011, **50**, 5870.
20 G. Demazeau, *J. Phys.: Condens. Matter.*, 2002, **14**, 11031.
21 X.G Zhao, T.T. Yan, K. Wang, Y. Yan, B. Zou, J.H. Y, R.R. Xu, *Eur. J. Inorg. Chem.*, 2012, 2527.
22 K. Kato, M. Sekita, S. Kimura, *Acta Crystallogr., Sect. B.*, 1979, **35**, 2201.
23 P.L. Chen, P.Y. Chiang, H.C. Yeh, B.C. Chang, K.H. Lii, *Dalton Trans.*, 2008, **13**, 1721.
24 P.L. Chen, P.Y. Chiang, H.Ch. Yeh, B.C. Chang, K.H. Lii, *Dalton Trans.* 2008, **51**, 1721.
25 C.H. Lin, C.S. Chen, A.A. Shiryaev, Y.V. Zubavichus, K.H. Lii, *Inorg. Chem.*, 2008, **47**, 4445.
26 C.H. Lin, R.K. Chiang, K.H. Lii, *J. Am. Chem. Soc.*, 2009, **131**, 2068.
27 Q.B. Nguyen, K.H. Lii, *Inorg. Chem.*, 2011, **50**, 9936.
28 Q.B. Nguyen , H.K. Liu , W.J. Chang , K.H. Lii, *Inorg. Chem.*, 2011, **50**, 4241.
29 G.M. Sheldrick, SHELXTL Programs, version 5.1, Bruker AXS GmbH, Karlsruhe, Germany, 1998.
30 G. Donnay, R. Allmann, *Am. Mineral.*, 1970, **55**, 1003.
31 R.C. Evans, D. Ananias, A. Douglas, P. Douglas, L.D. Carlos, J. Rocha, *J. Phys. Chem. C.*, 2008, **112**, 260.
32 D.J. Hou, H.B. Liang, M.B. Xie, X.M. Ding, J.P. Zhong, Q. Su, Y. Tao, Y. Huang, Z.H. Gao, Opt. Express., 2011, **19**, 11071
33 D.M. Fernandes, L.C. Silva, R.A.S. Ferreira, S.S. Balula, L.D. Carlos, B.D. Castro, C. Freire, *RSC Adv.*, 2013, **3**, 16697.
34 D.K, Cao, Y.H. Zhang, J. Huang, B. Liu, L.M, Zheng, RSC Adv., 2012, **2** , 6680.
35 C.F. Guo, H. Jing, T. Li, *RSC Adv.*, 2012, **2** , 2119.
36 W.R. Liu, C.H. Huang, C.W. Yeh, Y.C. Chiu, Y.T. Yeh, R.S. Liu, *RSC Adv.*, 2013, **3** , 9023.
37 L.L, Han, L. Zhao, J. Zhang, Y.Z. Wang, L.N. Guo, Y.H. Wang, *RSC Adv.*, 2013, **3** , 21824.